Chapter

Thermal and Mechanical Properties of Polypropylene Polymer Nanocomposites Infused with Sonochemically Coated SiC/SiO_2 Nanoparticles

Vijaya Rangari and James Davis

Abstract

This chapter describes the coating of silicon carbide nanoparticles on different types of silicon dioxide that varied in size and shape using sonochemical method. These composite particles were further infused into polypropylene polymer to increase its thermal and mechanical properties for various applications. A two-step process was used to fabricate SiC/SiO_2/polypropylene nanocomposites. In the first step, SiC nanoparticles were coated onto four different types of SiO_2 nanoparticles. The coated nanoparticles were then characterized using a high resolution transmission electron microscope (TEM), X-ray diffraction (XRD) determined the morphology and crystalline structure, and X-ray photoelectron spectroscopy (XPS). These results showed that the nanoparticles were crystalline, spherical in shape, and were uniformly coated. In the second step, nanocomposite samples were extruded using a Wayne Yellow Label Top single screw extruder. The as prepared nanocomposite samples were then characterized for their thermal and mechanical properties. These properties show increase in their flexural strength and thermal degradation. These results show increase in mechanical properties. The importance of this work lies in the simple sonochemical synthesis of SiC/SiO_2 hybrid nanomaterials and their filler applications in polypropylene polymer nanocomposites which are widely used for various application including automotive and electronic industries.

Keywords: polypropylene, melt extrusion, coating, ultrasound, mechanical properties

1. Introduction

In recent years, there have been rapid growth predictions for polypropylene-based composites, due to their applications in many fields such as automotive, home appliances, and construction industries [1–5]. Since the last decade, several nanoparticles have been incorporated into polypropylene and other thermoplastics as reinforcements, to produce stronger and lighter polymer composites [5–9]. There are many different thermoplastic polymers available on the market today such

as polypropylene, polyethylene, etc. Amongst these, polypropylene (PP) is one of the most widely used polymers due to the fact that it is inexpensive and offers attractive properties (rigidity, light weight, thermal and chemical stability, etc.); however, it has the disadvantage of being relatively brittle at room temperature and exhibiting poor resistance to crack propagation. Many investigations have been reported on fracture properties of polypropylene. It has thus been shown that fracture toughness of PP increases with increasing molecular weight and decreasing crystalline percentage. The temperature at brittle-ductile transition of PP has also been reported to increase with increasing crystallinity [10–13]. Most properties of polymers can be altered through the addition of fillers. Recent polymer nanocomposites have been an area of intense research because of their potential applications as multifunctional and high-performance materials. These nanocomposites are fabricated by simply adding small amounts of nanoparticles in the polymer matrices. The general class of nanocomposite is the mixture of organic and inorganic materials. Significant effort is focused on the ability to obtain control of the nanoscale structures via innovative synthetic approaches. This is a rapid growing area of research and is expanding as it generates many new exciting materials with various properties. These properties of nanocomposite materials depend not only on the properties but also on their morphology and interfacial characteristics. The nanoparticles significantly enhance the mechanical properties, thermal stability, reduced gas permeability, and other physicochemical properties [14–19] of the neat polymer. To change the properties of these composites, relatively small amounts of the nanoparticle are needed, more often the percentage by weight (0.5–5%) which results from the particles having incredibly high surface to volume ratios.

Since the discovery of nanoparticles, researchers are aiming to achieve a uniform particles-polymer interaction rather than the polymer-polymer or particle-particle interaction to obtain the maximum benefit. Wetzel et al. [20] incorporated various amounts of Al_2O_3 nanoparticles into a polymer matrix and studied the influence of nanoparticles on the flexural strength, impact energy, dynamic mechanical thermal properties, and block-on-ring wear behavior, and their results show the improvement in nanocomposites as compared to the neat polymer. Zheng et al. [21] employed high frequency ultrasonic and mechanical procedures to disperse spherical SiO_2 in epoxy resin. The results indicated that with the addition of 3 wt% of SiO_2 into the resin, the tensile strength improved by 114%, the stiffness improved by 13%, and the impact strength improved by 56%. Wang's et al. [22] reported that the dispersion of TiO_2 nanoparticles was coated by an acrylic acid (AA)-plasma-polymers in a glycol solution, and results indicated that the dispersion of TiO_2 nanoparticles were greatly improved after AA-plasma-polymer coating. They noted that the surface energy played a vital role in the dispersion behaviors of TiO_2 nanoparticles. It is an effective way to improve the dispersion of nanoparticles by changing their surface energy by plasma polymer coating. Dai et al. [23] synthesized β-SiC nanorods using the reaction of carbon nanotubes by using a mixture of Si and I_2 or through the use of a volatile SiO_2. In this study, there was a large quantity of β-SiC nanorods prepared which was wrapped with uniform amorphous SiO_2 layers on the outside surface. The formation of β-SiC nanorod was based on the carbothermal reduction of silica xerogels with carbon nanoparticles embedded in the network, and the formation of SiO_2 layer was from the reaction of decomposed SiO and O_2.

Extrusion is one of the most widely used processing techniques for fabrication of thermoplastic polymers. It can be used as a "stand alone" machine to directly shape parts or it can also be used as a melting device that is coupled with other secondary shaping devices. The two main advantages of this process over other manufacturing

processes are its ability to create very complex cross-sections and work materials that are brittle, because the material only encounters compressive and shear stresses. It also forms finished parts with an excellent surface finish [24, 25]. Extrusion is also used in the dispersion of nanoparticles to prepare polymer nanocomposites. Mohammed et al. [26] investigated the effect of SiO_2 infused into nylon-6 at wt% of 0, 1, and 2, respectively, and extruded into filaments. Experimental results showed that by infusing nanoparticles into nylon –6 and extruding it increased its tensile modulus, yield strength, hardening modulus, and ultimate tensile strength. There was a 45% enhancement in tensile modulus and a 26% enhancement in ultimate tensile strength observed in the 2 wt% system while compared to the neat nylon-6. TGA results indicated more thermal stability found in the nanophased infused systems, while the DSC studies indicated a more moderate increase in T_g. Liu et al. [27] presented the effects of incorporated montmorillonite (MMT) on a surface and the bulk mechanical properties of as-synthesized polyamide-6/montmorillonite (PA6/MMT) composites that were prepared using the twin-screw extruder mixing technique. Russo et al. [28] studied the effect of multiple extrusions on nanostructure and properties of nylon 6 nanocomposites. These researchers produced nanocomposites at different silicate loadings by melt compounding and submitted to further reprocessing by using single and twin screw extruders. Rheological, morphological, and mechanical analyses were carried out on as-produced and reprocessed samples to explore the influence of the number and the type of extrusion cycles on silicate nanodispersion. The results obtained displayed that the reprocessing by single screw extruder can modify the initial morphology since the re-agglomeration of the silicate layers can occur. However, a better nanodispersion was observed in the hybrids reprocessed by twin screw extruder, which was a result of the additional mechanical stresses able to realizing a dispersive mixing that contributes to avoid re-agglomeration phenomena. The high shear stresses produced with twin screw geometry determined also a significant degradation of neat matrix, principally based on chain scission mechanism. All as-produced and reprocessed hybrids showed a substantial enhancement in tensile modulus with the adding of silicate. However, the entity of performance enhancements displayed by the reprocessed hybrids was found to be highly dependent on the degradation of both organoclay and polymer matrix as well as the silicate amount, the number, and the type reprocessing. Investigations were made by Yong et al. [29] on the effects of the coating amount of surfactant and the particle concentration on the impact strength of polypropylene (PP)/$CaCO_3$ nanocomposites. These nanocomposites prepared with monolayer-coated $CaCO_3$ nanoparticles had the best mechanical properties, including Young's modulus, tensile yield stress, and impact strength because of the good dispersion of the nanoparticles in the polymer matrix, which in turn allowed them to study the effects of particle concentration on the impact strength of the nanocomposites. H-PP and E-PP, which were the low and high molecular weight PPs, respectively, were used as polymer matrices. Critical particle concentrations of 10 and 25 wt% corresponding to an abrupt increase in the impact toughness were determined for the E-PP and H-PP nanocomposites, respectively. Manolis et al. [30] observed a series of experiments which were performed on both simply supported and on-grade circular slab specimens, reinforced with different volumes of fibrillated polypropylene fibers in order to gauge its influence on the slab's impact resistance and natural frequency. Literature survey clearly suggests that there have been studies on polymer systems infused with nanofillers, but there are no reports on combination of silicon carbide, silicon dioxide coatings infused into polypropylene. Herein, this study we report the effects of reinforcement of silicon dioxide coated silicon carbide nanoparticles in polypropylene thermal and mechanical properties.

2. Experimental

2.1 Materials

The nanoparticles used in these experiments were spherical silicon carbide, ~30 nm in diameter. The β-silicon carbide nanoparticles were purchased from MTI Corporation, Richmond CA, USA. These nanoparticles were then coated with four different types of silicon dioxide nanoparticles, colloidal (Nissan chemicals), 80 nm, and areosil (Degussa), and needle shaped SiO_2 nanoparticles (Nissan chemicals). The colloidal silica solution MP-1040 was procured from Nissan Chemical Corporation. This filler is composed of 40% nanoparticles that are spherical in shape and approximately 200 nm in diameter dispersed in 60% of water. The 80 nm silica was procured from MTI Corporation Richmond CA, USA. These particles are spherical in shape having an 80 nm diameter. Areosil silica is also spherical in shape with a smaller diameter of approximately 5–15 nm and was also procured from Degussa. The other silica used was the needle shaped silica solution MP-1040 which was procured from Nissan Chemical Corporation. This filler is also composed of 40% nanoparticles and 60% water; however, these nanoparticles are irregular in shape.

2.1.1 Polypropylene

The matrix material used in this experiment is polypropylene procured from Chem Point. The polymer molecular weight ranged from 40,000 to 100,000, its powder diameter is approximately 20 μm, and the density of polypropylene is between 0.910 and 0.928 gr/ml. The melting point of polypropylene is 160°C with >50 isotactic crystalline structure. This type of high melting polymer can be molded or machined into structural components [31].

2.2 Synthesis of SiC/SiO_2 hybrid nanoparticles

In the first step, 250 mg of β-SiC was weighed and mixed along with 500 mg of powdered SiO_2, 250 mg of pluronic F-127 and 60 ml of ethylene glycol. The reaction mixture was irradiated using high intensity ultrasound for 3 hours at 5°C under argon gas flow. This process was done for each of the two powdered types of SiO_2; however for the solution types, when added to SiC nanoparticles, it was done using a weight ratio of 10:1. Upon completion of the sonication process, the silicon carbide coated silica nanoparticles were collected using a centrifuge at 12,000 rpm at 5°C for 30 min. The coated particles were washed 5 times, the first four times using distilled water and the last time with ethanol. The final step was to allow the sample to dry under vacuum for 24 hours at room temperature. Once dried, the coated nanoparticles were added to polypropylene at a ratio of 1:10 and then mixed using a Thinky mixer. The materials were placed in a special container and mixed under vacuum at 1200 rpm for 10 min. This step was done three times to ensure proper distribution of particles, before being extruded. This non-contact mixing method [32, 33] proves to be very efficient at dispersing nanofillers in polymer matrices without having any cross-contamination. This non-contact method works by independently revolving and rotating a container at various speeds in a planetary manner. As the container rotates, it experiences a number of forces that results in the material inside of the container being mixed. Centrifugal force presses the material outwards to the inner wall of the container, while other forces cause the material to move in a spiraling downwards direction along the slope of the container wall. The material then moves

back to the center of the container and up to the top repeating the process and in turn mixing the sample. As the material circulates from top to bottom, it generates a kneading effect forcing trapped air out of the material.

2.3 Extrusion

In the second phase, nanocomposites of polypropylene, silicon carbide/silicon dioxides were then extruded using a Wayne Yellow Label Top single screw extruder. The extruder has a 19 mm diameter screw, which is driven by a 2HP motor complete with a toothed timing belt for smooth speed reversal. Present are five thermostatically controlled heating zones that were used to melt the mixture before extrusion. Three of the zones were located inside the barrel and the final two were in the die zone set at respective temperatures of 340, 344, 350, 354, and 350°F. As the sample material passes through each zone, they are disintegrated into several branches and then combined again, which ensures proper distributive mixing of the nanoparticles and polypropylene. As the dispersed nanoparticles containing liquid polypropylene passes through the 10 cm long steel tube, it arrives to the die plate. As the sample passes through the extruder, it enters and completely fills the die, which in turn forms the flexure sample. The process schematic is shown in **Figure 1**.

2.4 Characterization

2.4.1 Transmission electron microscopy (TEM)

JOEL-2010, High Resolution (Japan), Transmission Electron Microscopy (HRTEM), is used to study the size, shape, and extent of coating of SiC onto SiO_2 nanoparticles. The samples were prepared by dispersing the nanoparticles in ethanol and placing a drop of the solution on a copper grid.

2.4.2 X-ray diffraction (XRD)

Rigaku D/MAX 2100 X-Ray Diffractometer (Japan) was used to study the structural characteristics. The samples were prepared for XRD by uniformly spreading the nanoparticles on a quartz sample holder. The test samples were conducted from 0 to 80° of two theta at room temperature. Characteristics XRD diffraction patterns were collected and matched with established data from PDF files. X-ray diffraction helps to determine the crystallographic configuration of the coated nanoparticles and its nanocomposites.

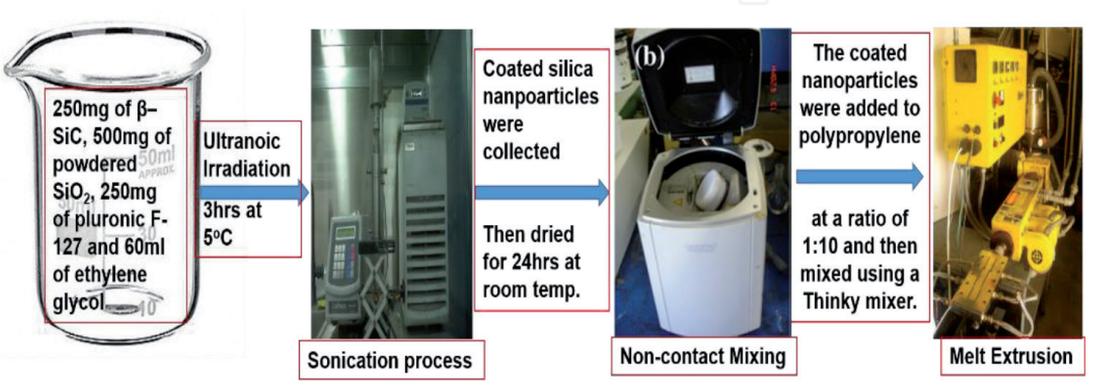

Figure 1.
Fabrication of polypropylene/SiC/SiO_2 nanocomposite.

2.4.3 X-ray photo electron spectroscopy (XPS)

This surface analysis technique (2–10 nm analysis depth typically) XPS can identify elemental composition, oxidation state, and chemical bonding like covalent bonds (oxides, nitrides, etc.) by evaluating binding energy shifts. This test was done at Cornell University Dr. Jonathan Shu's lab. The pressure in the analyzing chamber was typically 1.3×10^7 Pa under operating conditions. Photoelectrons were collected at approximately 45° from the specimen surface normal. The X-rays created photoemission electrons, and the signature of the photoemissions identified each element present in the samples.

2.4.4 Thermogravimetric analysis (TGA)

Thermogravimetric analysis was carried out using a Mettler Toledo (USA) TGA apparatus to find out the thermal stability of the test sample. This test is most commonly used to determine polymer decomposition temperatures, residual solvent levels, the amount of moisture content absorbed, and the amount of inorganic filler in polymer or composite material compositions. The samples were prepared by cutting the samples into small pieces, then placing 5 mg of the material in a platinum sample pan, and heating at a constant heating rate of 10°C/min from room temperature to 900°C under nitrogen atmosphere of 40 ml/min. The initial sample weight is measured at room temperature, and as heat is constantly being applied, the machine monitors the change in sample weight as a function of temperature. This result in weight loss versus temperature graphs being plotted from the data is obtained. In this case, the decomposition temperature is considered at 50% weight loss of the material.

2.4.5 Differential scanning calorimetry (DSC)

Differential scanning calorimetry (DSC) tests were carried out using a Mettler Toledo822^e (USA) from 30 to 300°C at a heating rate of 5°C/min under a nitrogen atmosphere then cooled from 300 to 30°C at the same rate. These results were used in measuring the melting temperature and the crystalline temperature.

2.4.6 Flexural analysis

Three-point bending flexural tests were conducted using a Zwick Roell MTS (Germany) to evaluate the samples flexural properties. Ten samples were tested using ASTM D790-03 testing standards which are of nominal size 100 mm (length) × 12.5 mm (width) × 5 mm (thick) and a span/thickness ratio maintained at 16:1. The test were conducted at room temperature at a constant crosshead speed of 2.0 mm/min. Stress-strain plots were obtained as the load displacement data were recorded through the data acquisition system equipped with the Zwick Roell MTS machine.

3. Results and discussion

3.1 X-ray diffraction (XRD)

XRD patterns were collected using a diffractometer operating in the Bragg-Brentano geometry utilizing Cu Kα radiation. The X-ray tube was operated at 40 kV and 30 mA. A 2θ scan range from 30 to 80° in steps of 2^0/min was recorded.

DOI: http://dx.doi.org/10.5772/intechopen.93498

The SiC coated onto various SiO_2 samples were analyzed to investigate the effects of ultrasonic irradiation on the nanoparticles. The XRD spectra of pure SiC can be seen below in **Figure 2(a)**. Through the use of the Jade 6.0 software, the peaks appearing at 2θ of 35.6, 41.5, 60.0, 72.0, and 75.5° indexed as (111), (200), (220), (311), and (222), designates the crystal spherical structured Moissanite-3C SiC (JCPDS 29-1129). The XRD of silicon carbide coating onto silicon dioxide was shown in **Figure 2(b)–(e)**, and it is evident that all of the SiC particles are crystalline in nature and all assigned to β-SiC. The background wide peak pattern is the characteristic of an amorphous SiO_2 phase. In the sample, the XRD data indicate the presence of only silicon carbide and amorphous silicon dioxide. The plot has characteristic peak intensities of FWHM, and d-spacing values which can be found in **Table 1**. A sharp peak around 35.6° corresponds to a spacing of 2.5189 A, which is attributed to the β-SiC (111) diffraction. There was an amorphous background present around 22° which is the result of the silicon dioxide presence. Deduced from the FWHM of β-SiC (111) diffraction peak. It is evident that, compared to pure SiC, the coated SiC FWHM peaks decreased significantly. In this case, the coated nanoparticles FWHM decreased compared to the neat, which results in coating of amorphous silica. The crystallite sizes of the particles were determined using Debye-Scherrer formula and FWHM method from the 100% peak of the pattern.

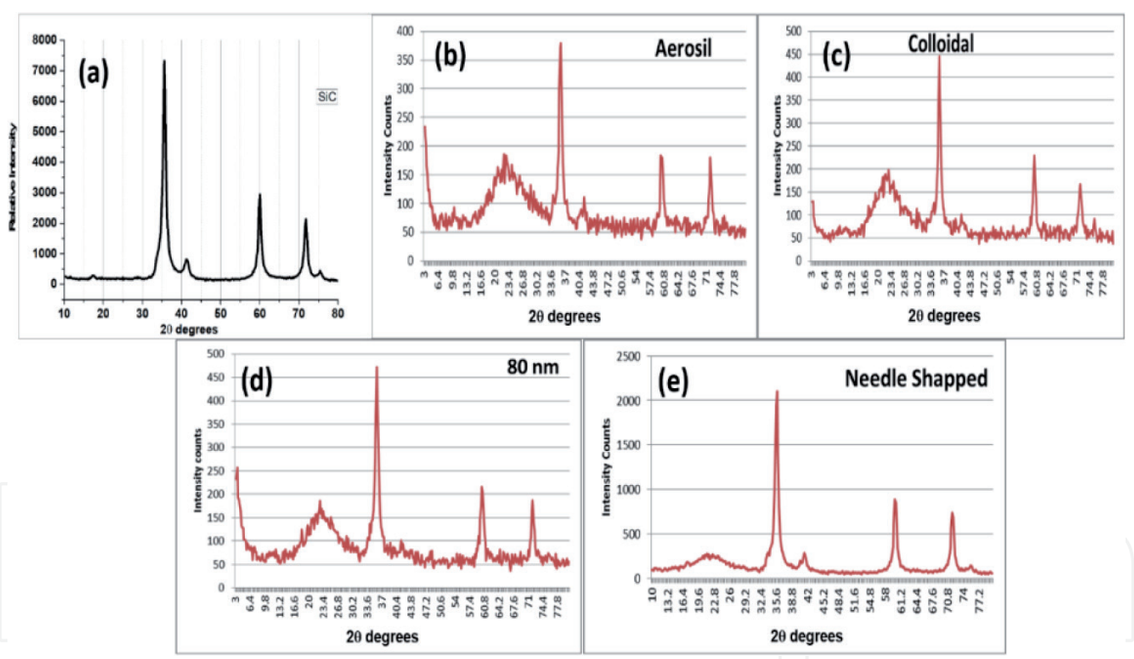

Figure 2.
XRD patterns of SiC and coated nanoparticles.

Sample	2θ at 100% intensity	FWHM(°)	FWHM at 35.6°
SiC	35.612	0.673	0.673
Colloidal	35.746	0.389	0.612
Areosil	35.813	0.397	0.604
80 nm	35.694	0.343	0.674
Needle shaped	35.865	0.368	0.652

Table 1.
XRD analysis of SiC and coated SiC, FWHM.

3.2 Transmission electron microscopy (TEM)

The TEM micrograph in **Figure 3** shows (a) as received SiC, (b) SiC coating on colloidal silica, (c) aerosol silica coated on SiC, (d) 80 nm silica coated on SiC, and finally (e) needle shaped silica coated on SiC. **Figure 3(a)** shows the SiC particles are spherical and particle sizes are about 30–50 nm. **Figure 3(b)** represents the coating of SiC on colloidal silica where the particles of silica are about 200 nm. The SiC particles are uniformly coated on silica spheres. **Figure 3(c)** shows that the particles of aerosol silica is coated on SiC nanoparticles. Since the aerosil silica is amorphous and also the particle sizes are about 5 nm, it is seen on the surface of SiC. In TEM **Figure 3(d)** and **(e)** shows the SiC particles and it was very hard to see the silica because of the silica is highly transparent to the electronic bean and difficult image.

3.3 X-ray photoelectron spectroscopy

XPS is a surface sensitive spectroscopic tool that provides information about chemical states and concentration of elements present in a sample with the exceptions of H and He. Each characteristic peak corresponds to the electron configuration of the electrons within the atoms, e.g., 1s, 2s, 2p, 3s, etc. This method uses soft X-rays to eject electrons from inner-shell orbital. The kinetic energy, E_k, of these photoelectrons is determined by the energy of the X-ray radiation, $h\nu$, and the electron binding energy, E_b, as given by:

$$E_k = h\nu - E_b - \emptyset \tag{1}$$

$$h \; - \; \text{Plank's constant} \; \left(6.62x10-34 \; J/s\right).$$

Using this technique, the surface of SiC and SiO_2 were characterized from the surface to approximately 10 nm in depth. Each element shows a characteristic set of peaks in the photoelectron spectrum at kinetic energies of the elemental

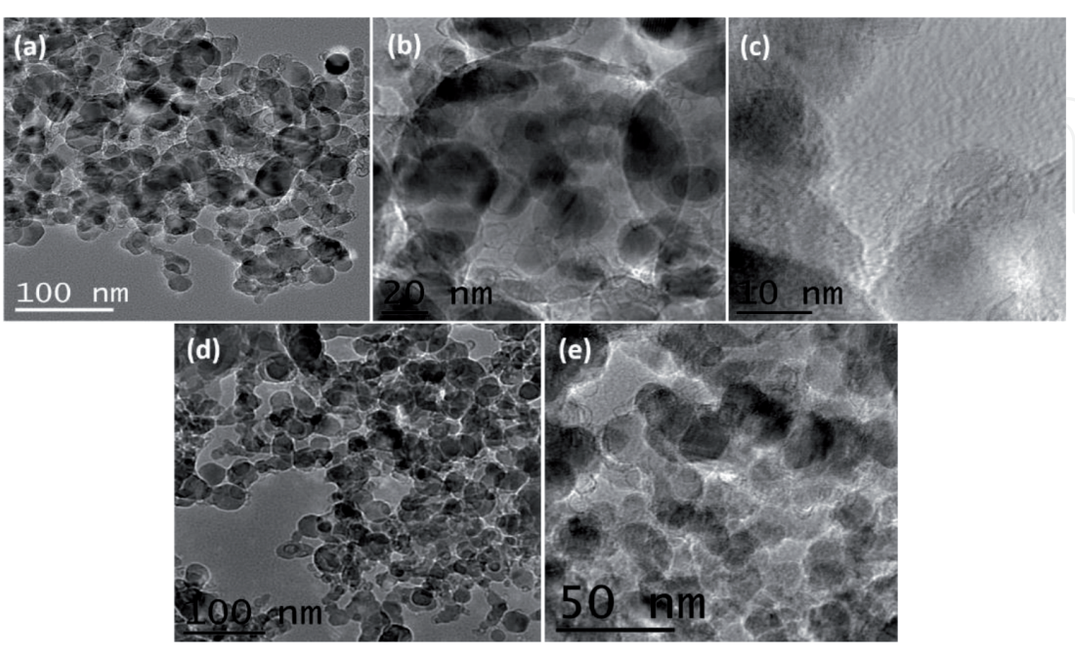

Figure 3.
TEM images of (a) SiC, (b) SiC coated SiO_2, (c) SiC coated areosil, (d) SiC coated needle SiO_2, and (e) SiC coated 80 nm SiO_2.

composition of the surface region determined by the photon energy and the respective binding energies. Elements exhibit binding energy peaks whose relative position depends on the electronegativity of their surrounding atomic neighbors. In the case of a phase mixture where more than one bonding state exists, a particular element is expected to have various binding energies, caused by different coordination/neighbor. The intensity of the peaks is related to the concentration of the element within the sampled region.

As shown in **Figure 4**, it displays the XPS spectra of SiC/SiO_2 nanomaterials. The most distinctive peaks present are the oxygen, carbon, and silicon peaks, respectively. Using the CasaXPS software for XPS analysis, a detailed spectrum of Si 2p, C 1s and O 1s of the chemical state of each element on the surface of the nanoparticles were identified and analyzed. Analysis of such element regions were done to confirm their attachment to the surface of the silicon dioxides. Silicon (Si 2p), carbon (C 1s), and oxygen (O 1s) elements can be found at binding energies of 102.8, 284.6, and 532.0 electron volts (eV), respectively. Also in **Figure 4** above, one can take a look at the as received SiC which clearly shows a Si peak, but also shows where adsorbed contaminations like oxygen and carbon were found on the top layer within about 6 nm in thickness. This observation is consistent with other researchers [34, 35] and can be a result of the absorption of atmospheric oxygen. **Figure 5(a)** shows the high resolution scan of the deconvoluted XPS spectra of neat SiC for Si 2p peak and C 1s on the sub-surface layer. The spectra were Gaussian fitted based on the published data of the binding energies. The spectra emission line at binding energy (BE) of 100.47 eV is associated with the SiC bonding. In addition to this, two more fitted chemical shifts were observed at BE of 98.4 and 102.9 eV, which were identified as Si° and SiO_2, respectively, for the spectra of SiC for Si 2p peak.

For the spectra of SiC, the C 1s spectrum was deconvoluted into three peaks (**Figure 5(b)** of BE 285.5, 282.7, and 289.06eV. The peak at 285.5 eV signified the presence of carbon in the form of hydrocarbon, while the peak at 282.7 eV is due to the binding energy of carbon in the form of SiC, and in the form of carbon bonded to oxygen, this was observed at 289.06eV. The binding energy for oxygen or O 1s was found to be 532.6 eV and can be associated either with O_2-Si or C-O bonding which can be a result of surface contamination. From the surface chemical composition, it can be seen that the ratio of Si/C was found to be 0.29, which is much lower than the theoretical value for pure SiC of 0.5 which clearly indicates surface contamination.

The coated hybrid nanocomposites of colloidal, areosil, 80 nm, and needle shape nanocomposites were also investigated using XPS for comparison with the neat sample. The chemical composition and binding energies were tabulated and

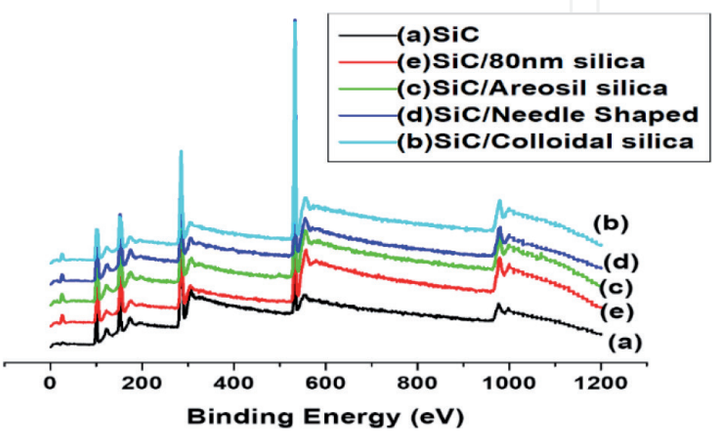

Figure 4.
XPS spectra for neat SiC and coated nanoparticles.

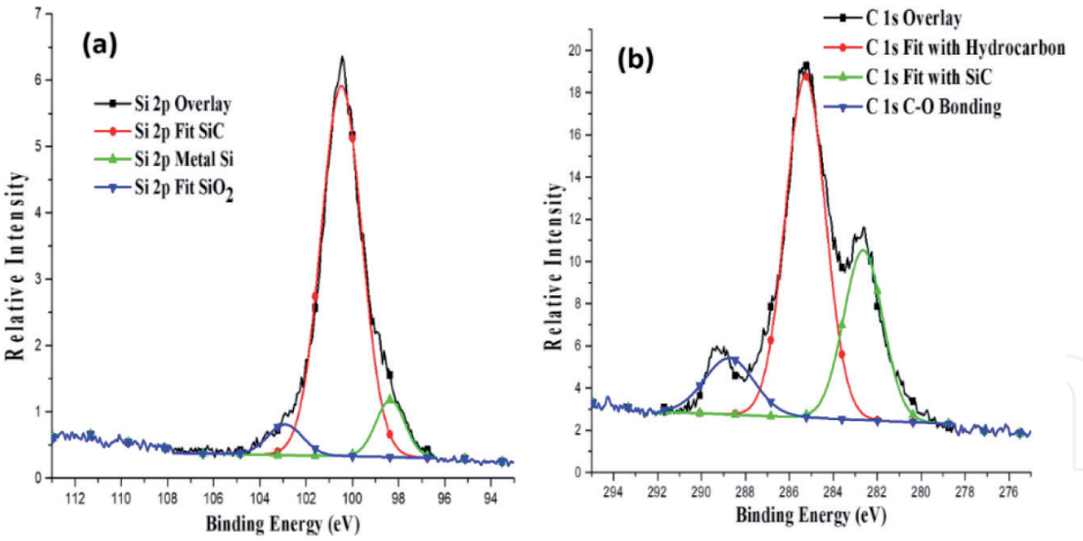

Figure 5.
Deconvoluted XPS spectra for SiC for (a) Si 2p peak (b) C 1s peak.

presented in **Table 2**. The O/Si ratios from the table obviously doubled which indicated that surface contaminant oxygen was increased when SiC was sonicated with the four different types of SiO_2. The concentration of C in the near surface decreases from 65.09% for neat SiC to an average of 43.26% for sonicated SiC in SiO_2. This decrease is may be removal of carbon in the form of CO_2. However, it can be seen here that, the as received SiC absorb oxygen which is enough to impart strong chemical double bonding in the system.

Figures 6–9 depict the deconvoluted XPS spectra for peaks Si 2p, C 1s, and O 1s of the coated samples of colloidal, areosil, needle shaped and 80 nm nanoparticles. For each of the nanoparticles samples made using high intensity ultrasound irradiation, there were noticeable chemical shifts in peak observed indicating the coating of SiC onto SiO_2 nanoparticles that took place. This was further confirmed from the elemental concentration at the surface. These spectra could be separated into two or three peaks based on the assumption that each peak consists of the Gaussian/Lorentzian sum function. The Si(2p) peak was separated into the Si–Si, Si–C, and SiO_x peaks, and the C(1s) peak was decomposed into the C–Si, C–C, C–O–H, and C=O peaks [34–39]. The energy positions of these peaks are listed in **Table 3**. The separation of the elements is not sufficient to precisely obtain the fraction of the bond. Therefore, as a rough estimation, the fraction of the bond was obtained from the ratio of the area of each peak [40]. The FWHM of Si–Si and Si–C are 2.13 and 1.38 eV, respectively. The FWHM of C–C and C=C are 2.1 and 1.2 eV, respectively. The ratio between C–C and C=C bond concentration is 10.1.

Samples	Composition (atomic %) at the surface of nanoparticles			Atomic ratios of O/Si
	Si	O	C	
As received SiC	19.05	15.86	65.09	0.83
Colloidal	20.91	33.64	45.45	1.60
Areosil	23.59	34.51	41.35	1.46
80 nm	19.82	37.28	42.90	1.88
Needle shaped	25.66	30.97	43.37	1.20

Table 2.
Surface chemical composition of neat SiC and coated nanoparticles.

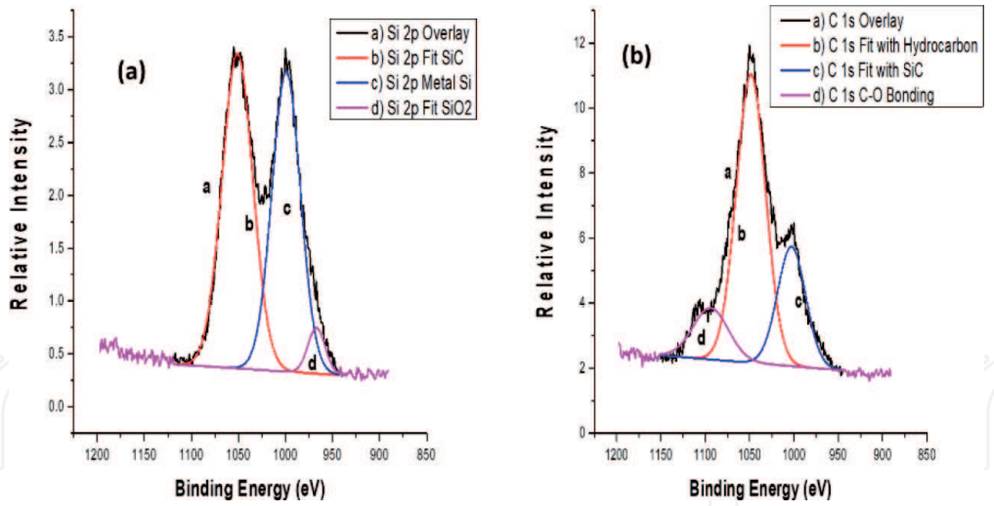

Figure 6.
Deconvoluted XPS spectrum of SiC/SiO_2 (colloidal) for Si 2p peak and C 1s.

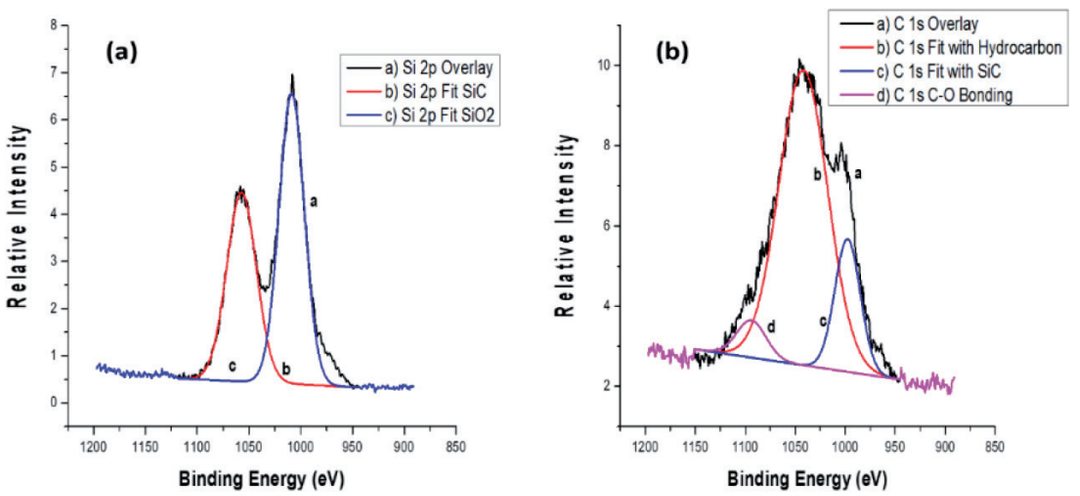

Figure 7.
Deconvoluted XPS spectrum of SiC/SiO_2 (Areosil) for (a) Si 2p peak and (b) C 1s.

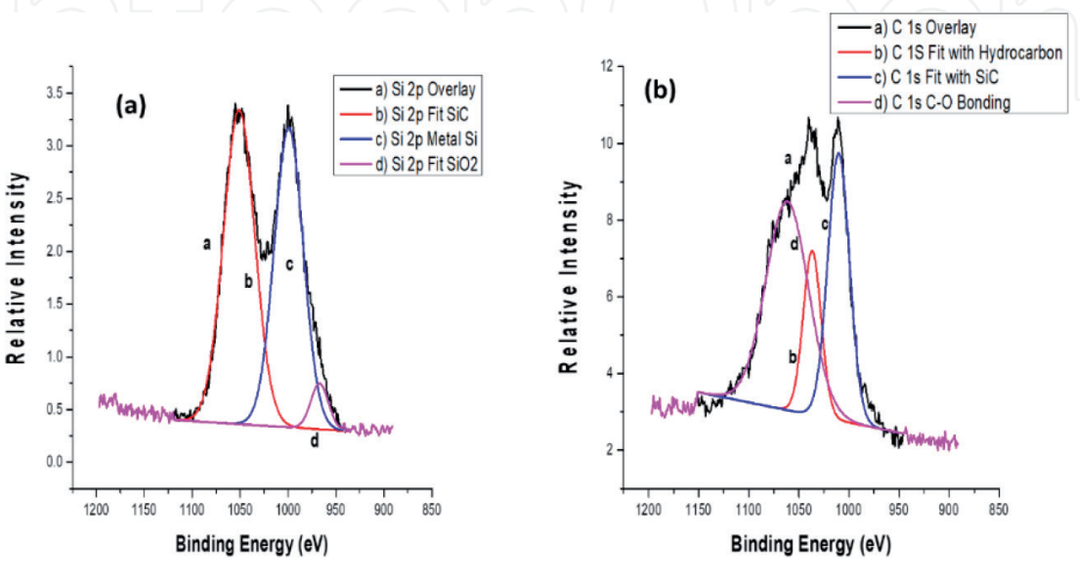

Figure 8.
Deconvoluted XPS spectrum of SiC/SiO_2 (needle shape) for (a) Si 2p peak and (b) C 1s.

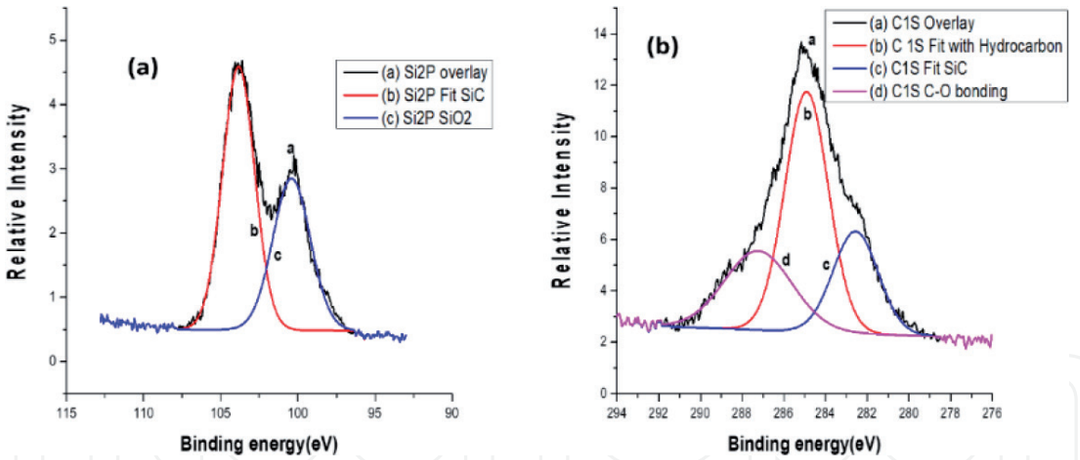

Figure 9.
Deconvoluted XPS spectra of SiC/SiO_2 (80 nm) for (a) Si 2p and (b) C 1s.

Bond	Binding energy (eV)
Si–Si	99.2
Si–C	100.5
O–Si–C	101.8
SiO_x	103.2
C–Si	283.2
C–C	284.6
C–O–H	286.4
C=O	288.4

Table 3.
Binding energy of different bonds.

The deconvoluted XPS spectrum of SiC/SiO_2 (Colloidal) for Si 2p peak and C 1s is shown in **Figure 5**. Similar results were obtained such as, the BE of 103.35, 99.99, and 97.91 eV that were associated with SiO_x, Si–C, and Si–Si bonding, respectively, for Si 2p. Fitted curve for C 1s also showed similar results of C–C and C–Si bonding occurring. The O 1s emission was also found at BE of 532.55 eV. The surface chemical composition of Si, O and C obtained from CasaXPS were 20.91, 33.64 and 45.45, respectively.

The deconvoluted XPS spectrum of SiC/SiO_2 (Areosil) for Si 2p peak and C 1s is shown in **Figure 7**. The BE was found to be 103.48 and 100.089 eV for Si 2p which are associated with SiO_x bonding and Si–C bonding, respectively. Whereas, fitted curve for C 1s at 284.76 and 282.88 eV of BE was indicating the C–C and C–Si bonding. The O 1s emission was found at BE of 532.55 eV, and the surface chemical composition of Si, O, and C obtained from CasaXPS were 23.59, 34.51, and 41.35%, respectively. There was evident of small amounts of Na 1s present that accounted for the remaining 0.56% of the chemical composition. This was believed to be the result of surface or apparatus contamination.

Figure 8 shows the deconvoluted XPS spectrum of SiC/SiO_2 (needle shape) for Si 2p peak and C 1s. The BE was found to be associated with Si–C bonding at 100.61 eV, Si–Si at 98.35 and 103.74 eV related with Si–O bonding, respectively, for Si 2p. Fitted curve for C 1s was also obtained at 284.46 and 283.02 eV of BE was indicating the C–C and the Si–C bonding. In addition to these, the O 1s emission

was also found at BE of 532.55 eV. The surface chemical composition of Si, O, and C obtained from CasaXPS were 25.66, 30.97, and 43.37%, respectively.

Figure 9 depicts the deconvoluted XPS spectrum of SiC/SiO_2 (80 nm) for Si 2p peak and C 1s. The BE was found to be associated with Si–C bonding at 100.41 and 103.84 eV related with Si–O bonding, respectively, for Si 2p. On the other hand, fitted curve for C 1s at 284.76 and 282.28 eV of BE was indicating the C–C and the Si–C bonding. In addition to these, the O 1s emission was found at BE of 532.55 eV. The surface chemical composition of Si, O, and C obtained from CasaXPS was 19.82, 37.28 and 42.90 respectively.

The observed shift in the Si 2p peak between the oxide and the carbide is consistent with the expected change in oxidation state. Additional information on the interface was obtained from the C 1s photoelectron spectrum of the nominally bare SiC, far from the interface as shown in **Figure 10**. The narrow second highest energy peak is the expected C 1s signal from bulk SiC [41]. From the observed chemical shifts, we can determine the ionic state of a particular species. Although the incident X-rays penetrate deep into the sample, only electrons emitted from a thin surface layer are detected. The electron escape depth for Si, C, and O ranges from 2.0 to 2.5 nm [42].

3.4 Differential scanning calorimetry (DSC)

Differential scanning calolimetry (DSC) is a thermoanalytical technique by which the energy absorbed or emitted by the material as a function of temperature or time is measured. In present case, we have studied the extruded-polymer nanocomposites to determine the thermal transitions such as the melting (T_m) of a crystalline polymer as shown in **Figure 11**. The DSC data are presented in **Table 4**.

The curve shapes of the neat material and nanocomposites are very similar, with only slight differences in the leading edge of the melt peak, indicating that the neat structure has little effect on the overall phase structure of the material. Above the melting temperature of about 160°C, the polymer is subject to a thermal degradation that is both dependent on time and on temperature. Adding nanoparticles allow the start of the degradation process to shift toward higher temperatures. The increase of the melting temperature of neat PP to PP + SiC was 161.43–166.12°C. Correlation has also been drawn between orientation (crystal perfection) and the DSC melt peak temperature [43].

The crystallization peak temperatures are shown below in **Figure 11**; they follow the same order as the melt peak temperatures, with the neat pp material being more

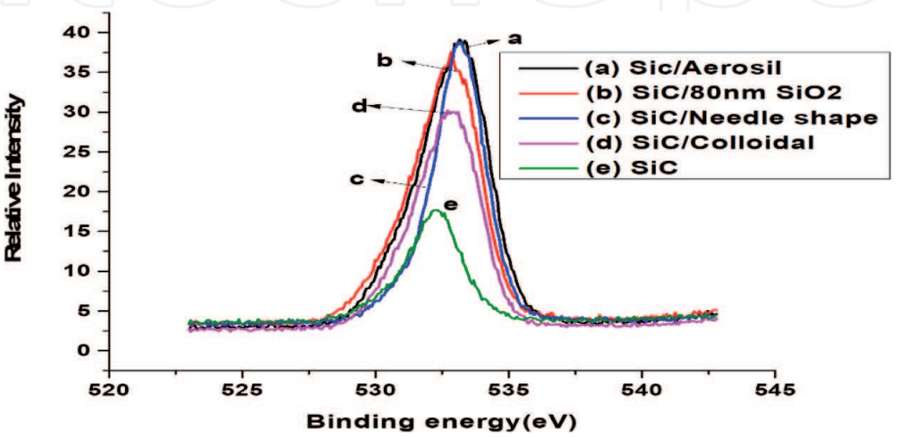

Figure 10.
XPS overlay of O 1s binding energy for SiC and the coated nanoparticles.

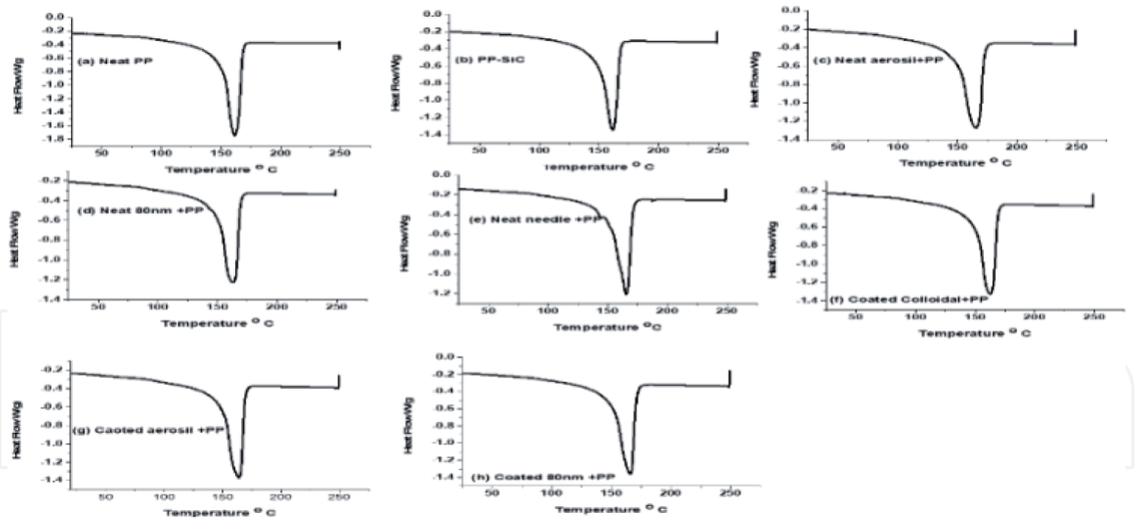

Figure 11.
DSC melting curve of neat PP and nanocomposites.

easily crystallizable. Preliminary isothermal crystallization studies at 116°C of neat polypropylene also show a similar trend. A decrease in the crystallization temperature after introduction of the filler indicates that a higher undercooling of the melt is necessary for the crystallization to occur. Such behavior may be the result of the strong influence of the SiC/SiO_2 nanoparticles on the chain dynamics (lower chain mobility). It has been shown that the crystallization rate increases as both molecular weight and molecular weight distribution increase [44].

Several authors have seen multiple melting peaks in polypropylene, and there is the suggestion of multiple crystalline forms in the polypropylene [33, 44, 45]. It is alternatively suggested that the low temperature melting is caused by a less perfect crystalline order and not from different crystal phases [46]. With very sharp crystallization peaks, it is likely that the low temperature phase is induced at the crystallization temperature. Similar phenomena have been observed for isothermal crystallization [47] and this probably explains the difference in peak temperature between the nanocomposites. It is also plausible that the different polymer fractions do not co-crystallize simultaneously, and that the lower temperature melts is due to morphological effects. It is possible that the higher melt temperature of neat PP implies the molecular weight of the nanocomposites is greater than the neat PP (**Table 4**).

Sample	Melting temperatures (°C)	Crystallization temperatures (°C)
Pure PP	161.43	113.72
Neat areosil	165.48	111.12
Neat 80 nm	163.16	112.83
Neat needle shape	165.60	111.31
PP + SiC	161.51	116.80
Coated areosil	166.12	113.20
Coated colloidal	162.84	113.54
Coated 80 nm	163.70	111.72

Table 4.
DSC melting and crystallization temperature chart.

3.5 Thermogravimetric analysis (TGA)

The applications of TGA are to determine the absorbed moisture content, residual solvent levels, the amount of inorganic filler in a polymer, and in this case the degradation characteristics of the coated nanocomposites in terms of their induction time. The weight loss of a polymer as a function of temperature is commonly determined by this technique. Weight loss of a polymer due to thermal degradation is an irreversible process. Such thermal degradation is largely related to oxidation whereby the molecular bonds of a polymer are attacked by oxygen molecules. **Figure 12** is the TGA graph of extruded neat silicon carbide coating with polypropylene and extruded samples of coated nanoparticles with polypropylene. The TGA data are presented in **Table 5**.

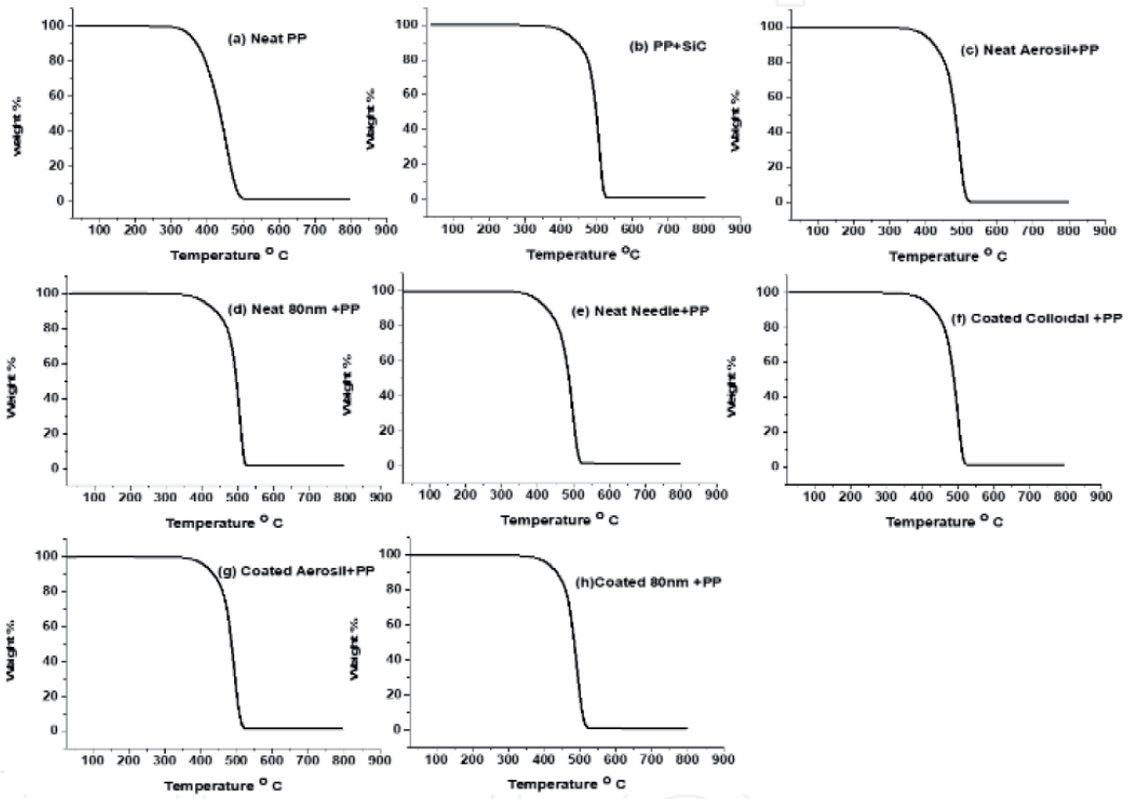

Figure 12.
TGA curves of neat and SiC/SiO_2 reinforced polypropylene nanocomposite.

Sample	T_d (°C)	T_{50} (°C)	% Temperature increase
Pure PP	369.78	436.06	—
Neat areosil	452.94	488.59	12.0
Neat 80 nm	469.68	496.34	13.8
Neat needle shape	464.94	493.48	13.1
PP + SiC	453.67	483.60	10.9
Coated areosil	454.06	486.11	11.4
Coated colloidal	446.79	487.50	11.7
Coated 80 nm	447.71	482.39	10.6

Table 5.
Parameters obtained from TGA curves.

In the present study, TGA results show that 50% of the total weight loss is considered as the structural destabilization point of the system. It is a common practice to consider 50% weight loss as an indicator for structural destabilization. From **Figure 12**, it is evident that the neat sample is stable up to 436.06 °C, whereas the coated nanocomposites minimum stabilization temperature is at 482.39°C which is a 10.6% increase. The maximum temperature increase was 13.8% and stabilization occurred at 496.34°C for the neat 80 nm sample. The reason for this increase in the thermal stability is due to the increase in cross-linking of the coated nanoparticles in the presence of polypropylene and having minimum particle to particle interaction.

This may be due to the presence of silicon carbide nanoparticles which are high heat absorbing materials compared to neat polypropylene, which can be the reason for having such a positive impact on improving the decomposition temperature. One can also assume that the nanoparticles were well dispersed and were not acting as impurities in agglomerated form due to the increase. Another probable reason for the observed behavior could be the lower mobility of the polymer chains due to strong interaction with the nanofiller. Thermal degradation of polypropylene begins with formation of the free radicals, which further induce chain fragmentation processes [48]. Volatile oligomers that are formed which are responsible for the mass loss will be partially prevented which results in the whole degradation process to shift towards a higher temperature.

3.6 Flexural test

The flexure test method measures behavior of materials subjected to simple beam loading. It produces tensile stress in the convex side of the specimen and compression stress in the concave side which creates an area of shear stress along the midline.

Flexure stress-strain curves for neat polypropylene and the nanocomposites are shown in **Figure 13**. The flexural test data are presented in **Table 6**. From the graph, it is evident that flexural strength and modulus slightly increases with the addition of coated SiC/SiO_2 nanofillers with respect to the neat polymer. In the table, we see that coated colloidal contributed the maximum percent change in stiffness at 40.5%, while the coated 80 nm contributed to a maximum strength percent change

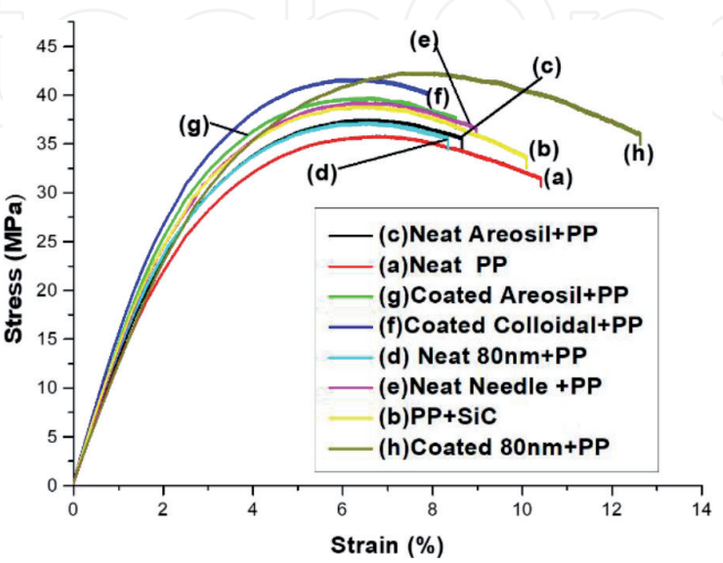

Figure 13.
Stress-strain curve from flexure results.

Sample	Strength (MPa)	% Strength change	Modulus	% Modulus change	Strain (%)	% Increase in toughness
Pure PP	33.97	—	1.16	—	7.09	—
Neat areosil	35.82	5.4	1.31	12.9	6.83	13.2
Neat 80 nm	37.50	10.3	1.42	22.4	6.65	22.4
Neat needle shape	39.76	17.0	1.48	27.5	6.61	27.5
PP + SiC	38.88	14.4	1.45	25	6.50	25
Coated areosil	39.26	15.5	1.49	28.4	6.29	30.1
Coated colloidal	41.65	22.6	1.63	40.5	6.48	41.5
Coated 80 nm	42.33	24.6	1.28	10.3	7.29	92.4

Table 6.
Mechanical properties from flexure test.

at 24.6%, and the greatest toughness percent change which was at 92.4%. Although these were the highest values observed, it is still evident that overall, all of the samples performed greater than the neat PP sample.

The reason for such change in stiffness of the matrix is due to ultrasound irradiation which enhances the homogeneity. The ultrasound irradiation helps in molecular mixing of these components together and the formation of coated reactive particles which ultimately leads to increase the cross-linking in the polymer when mixed. The decrease in mobility of the cross linking in polymer gives better mechanical properties with an optimum amount of nanofiller addition. Surface area also played an important role in the significant increase in that the spherical spatial distribution and low weight ratio of the nanofillers enhance the homogeneity of the reaction. The nanocomposites exhibit ductile fracture and the elongation at break increased with the increase of the nanoparticle content (**Table 6**).

4. Conclusion

The samples were prepared using high intensity ultrasound irradiation to coat SiC onto SiO_2 nanoparticles. This process has been introduced as an efficient way to disperse SiC onto SiO_2 nanoparticles, and by extruding these samples with polypropylene, it increases its mechanical properties. XRD analysis confirmed that the samples were crystalline with an amorphous background present. The TEM analysis revealed that the SiC nanoparticles were uniformly dispersed over the entire surface of the SiO_2 nanoparticles. It also indicated a minor growth in the size of the nanoparticles after ultrasonic irradiation. XPS spectrographs revealed the chemical composites found in the samples. It also verified the surface coating through the shifts in binding energies. The crystallization of the polypropylene polymer matrix was also affected by the presence of the coated nanoparticles. DSC testing indicated that the crystallization and the melting temperatures increased with increasing filler content. Through DSC, it can be seen that by adding nanoparticles, it allows the start of the degradation process to shift toward higher temperatures. The increase of the melting temperature of neat PP to PP + SiC was 161.43–166.12°C. A decrease in the crystallization temperature after introduction of the filler indicates that a higher undercooling of the melt is necessary for the crystallization to occur.

The TGA data showed that the neat sample is stable up to 436.06°C, whereas the coated nanocomposites minimum stabilization temperature is at 482.39°C which is a 10.6% increase. The maximum temperature increase was 13.8% and stabilization occurred at 496.34°C for the neat 80 nm sample. The coated nanocomposites had profound effects on the PP properties. The flexure test results showed that the flexural strength and modulus slightly increases with the addition of coated SiC/SiO_2 nanofillers with respect to the neat polymer.

Acknowledgements

The authors acknowledge the financial support of NSF-RISE # 1459007, NSF-CREST#1735971 and NSF-MRI-1531934 grants.

Conflict of interest

The authors declare no conflict of interest.

Author details

Vijaya Rangari* and James Davis
Department of Materials Science and Engineering, Tuskegee University, Tuskegee, Alabama, USA

*Address all correspondence to: vrangari@tuskegee.edu

References

[1] Wei S, Xu L, Shen Y, Zhang L, Wu X. Study on microscopic mechanism of nano-silicon dioxide for improving mechanical properties of polypropylene. Molecular Simulation. 2020;**46**(6):468-475

[2] Awad AH, El-Gamasy R, Abd El-Wahab AA, Abdellatif MH. Mechanical behavior of PP reinforced with marble dust. Construction and Building Materials. 2019;**228**:116766

[3] Massoud GB, Carl D, Denis R. Mechanical, water absorption, and aging properties of polypropylene/flax/glass fiber hybrid composites. Journal of Composite Materials. 2015;**49**:3781-3798

[4] Lule ZC, Kim J. Thermally conductive polybutylene succinate composite filled with Si-O-N-C functionalized silicon carbide fabricated via low-speed melt extrusion. European Polymer Journal. 2020;**134**(5):109849

[5] Biswas MC, Tiimob BJ, Abdela W, Jeelani S, Rangari VK. Nano silica-carbon-silver ternary hybrid induced antimicrobial composite films for food packaging application. Food Packaging and Shelf Life. 2019;**19**: 104-113

[6] Akpan EI, Shen X, Wetzel B, Friedrich K. Design and synthesis of polymer nanocomposites. In: Polymer Composites with Functionalized Nanoparticles Synthesis, Properties, and Applications, Micro and Nano Technologies. Elsevier; 2019. pp. 47-83

[7] Damian Beasock T, Stokes M, El-Ghannam A, Schmitz T. Effect of processing parameters on the microstructure and mechanical behavior of a silicon carbide-silica composite. Procedia Manufacturing. 2019;**34**:747-753

[8] Imam MA, Jeelani S, Rangari VK. Thermal decomposition and mechanical characterization of poly (lactic acid) and potato starch blend reinforced with biowaste SiO_2. Journal of Composite Materials. 2019;**53**:2315-2334

[9] Mekuria TD, Zhang C, Fouad DE. The effect of thermally developed SiC@SiO_2 core-shell structured nanoparticles on the mechanical, thermal and UV-shielding properties of polyimide composites. Composites Part B: Engineering. 2019;**173**:106917

[10] Abdel-Hamid IM. Thermo-mechanical characteristics of thermally aged polyethylene/polypropylene blends. Materials and Design. 2010;**31**:918-929

[11] Greco R, Ragosta G. Isotactic polypropylene of different molecular characteristics: Influence of crystallization conditions and annealing on fracture behavior. Journal of Materials Science. 1988;**23**:4171-4180

[12] Ouderni M, Philips PJ. Influence of morphology on the fracture toughness of isotactic polypropylene. Journal of Polymer Science. Part B. 1995;**33**:1313-1322

[13] Thumm A, Risani R, Dickson A, Sorieul M. Ligno-cellulosic fibre sized with nucleating agents promoting transcrystallinity in isotactic polypropylene composites. Materials. 2020;**13**:1259

[14] Ščetar M, Kurek M, Režek JA. Effect of high power ultrasound on physical–chemical properties of polypropylene films aimed for food packaging: Structure and surface features. Polymer Bulletin. 2019;**76**:1007-1021

[15] Liang J-Z. Effects of tension rates and filler size on tensile properties of polypropylene/graphene nano-platelets

composites. Composites Part B Engineering. 2019;**167**:241-249

[16] Kulkarni MB, Radhakrishnan S, Samarth N, Mahanwar PA. Structure, mechanical and thermal properties of polypropylene based hybrid composites with banana fiber and fly ash. Materials Research Express. 2019;**6**:075318

[17] Ibhadon O. Fracture mechanics of polypropylene: Effect of molecular characteristics, crystallization conditions, and annealing on morphology and impact performance. Journal of Applied Polymer Science. 1998;**69**:2657-2661

[18] Friedrich K. Strength of crystalline isotactic polypropylene and the effect of molecular and morphological parameters. Progress in Colloid and Polymer Science. 1979;**66**:299-309

[19] Van der Wal A, Mulder JJ, Gaymans RJ. Fracture of polypropylene: The effect of crystallinity. Polymer. 1998;**39**:5477-5481

[20] Wetzel B, Haupert F, Zhang MQ. Epoxy nanocomposites with high mechanical and tribological performance. Composites Science and Technology. 2003;**63**:1-13

[21] Zheng Y, Zheng Y, Ning R. Effect of nanoparticles SiO_2 on the performance of nanocomposites. Materials Letters. 2003;**57**:2940-2944

[22] Ying W, Jing Z, Xinyuan S, Changnian S, Jiajun W, Li S. Dispersion investigation of TiO_2 nanoparticles coated by pulsed RF plasma polymer. Materials Chemistry and Physics. 2006;**98**:217-224

[23] Dai H, Wong EW, Lu YZ, Fan SS, Lieber CM. Synthesis and characterization of carbide nanorods. Nature. 1995;**374**:769-772

[24] Bralla JG, editor. Handbook of Product Design for Manufacturing. New York: McGraw-Hill Publishing Company; 1986

[25] Wick C, Benedict JT, Veilleux RF. Tool and Manufacturing Engineers Handbook. 4th ed. Vol. 2. Society of Manufacturing Engineers (SME); 1984. ISBN: 0-87263-135-4

[26] Hassan M, Zhou Y, Mahfuz H, Jeelani S. Effect of SiO_2 nanoparticles on thermal and tensile behavior of nylon-6. Materials Science and Engineering A. 2006;**429**:181-188

[27] Sung-Po L, Shyh-Shin H, Jui-Ming Y, Chi-Chang H. Mechanical properties of polyamide-6/ montmorillonite nanocomposites. Prepared by the twin screw extruder mixed technique. International Communications in Heat and Mass Transfer. 2011;**38**(1):37-43

[28] Russo GM, Nicolais V, Di Maio L, Montesano S, Incarnato L. Rheological and mechanical properties of nylon 6 nanocomposites submitted to reprocessing with single and twin screw extruders. Polymer Degradation and Stability. 2007;**92**:1925-1933

[29] Yong L, Haibin C, Chi-Ming C, Jingshen W. Effects of coating amount and particle concentration on the impact toughness of polypropylene/ $CaCO_3$ nanocomposites. European Polymer Journal. 2011;**47**:294-304

[30] Manolis GD, Gareis PJ, Tsono AD, Neal JA. Dynamic properties of polypropylene fiber-reinforced concrete slabs. Cement and Concrete Composites. 1997;**19**(4):341-349

[31] Xiangmeng L, Ming K, Lu Y, Simin S, Rong S, Lixian S, et al. Quantitative evaluation of fillers dispersion state in $CaCO_3$/polypropylene composites through visualization and

fractal analysis. Polymer Composites. 2020;**41**:1605-1613

[32] Vijaya KR, Tarig AH, Quentin M, Shaik J. Size reduction of WO_3 nanoparticles by ultrasound irradiation and its applications in structural nanocomposites. Composites Science and Technology. 2009;**69**:2293-2300

[33] Vijaya KR, Mohammad SB, Shaik J. Microwave processing and charactering of EPON 862/CNTs nanocomposites. Materials Science and Engineering B. 2010;**168**:117-121

[34] Margiotta JC. Study of silicon carbide formation by liquid silicon infiltration of porous carbon structures [PhD dissertation]. Baltimore, MD, USA: The Johns Hopkins University; 2009

[35] Solomon I, Schmidt MP, Senemand C, DrissKhodja M. Band structure of carbonated amorphous silicon studied by optical, photoelectron, and X-ray spectroscopy. Physical Review B. 1988;**38**:13263

[36] Lee WY. X-ray photoelectron spectroscopy and Auger electron spectroscopy studies of glow discharge $Si_{1-x}C_x$:H films. Journal of Applied Physics. 1980;**51**:3365

[37] Choi WK, Loo FL, Loh FC, Tan KL. Structural and electrical studies of radio frequency sputtered hydrogenated amorphous silicon carbide films. Journal of Applied Physics. 1995;**78**:7289

[38] Demichelis F, Giorgis F, Pirri CF, Tresso E. Bonding structure and defects in wide band gap a-Si_{1-x} C $x_{:H}$ films deposited in Hz diluted SiH_4 + CH_4 gas mixtures. Philosophical Magazine B. 1995;**71**:1015

[39] Demichelis F, Crovin G, Pirri CF, Tresso E, Rava P, Gallini R, et al. Optimization of relevant deposition parameters for high quality a-SiC:H films. Solar Energy Materials & Solar Cells. 1995;**37**:315

[40] Katiyar M, Yang YH, Abelson JR. Si–C–H bonding in amorphous $Si_{1-x}C_x$:H film/substrate interfaces determined by real time infrared absorption during reactive magnetron sputter deposition. Journal of Applied Physics. 1995;**78**:1659

[41] Muehlhoff L, Choyke WJ, Bozack MJ, Yates JT. Comparative electron spectroscopic studies of surface segregation on SiC(0001) and SiC(0001). Journal of Applied Physics. 1986;**60**:2842

[42] Himpsel FJ, McFeely FR, Taleb-Ibrahimi A, Yarmoff JA. Microscopic structure of the SiO_2/Si interface. Physical Review B. 1988;**38**:6084

[43] Jaffe M, Turi E, editors. Thermal Characterization of Polymeric Materials. New York: Academic Press; 1981. pp. 731-781

[44] Ahmed M. Polypropylene Fibers - Science and Technology. New York: Elsevier; 1982. p. 187

[45] Saraf AW, Desai P, Abhiraman AS. Applied Polymer Symposium 47. New York: Wiley; 1991. p. 67

[46] Caldas V, Brown GR, Nohr RS, Macdonald JG, Taboin LE. The structure of the mesomorphic phase of quenched isotactic polypropylene. Polymer. 1994;**35**:899

[47] Crompton TR. Thermal Methods of Polymer Analysis. Smithers Rapra Technology; 2013. ISBN-10:1847356621

[48] Allen NS, Edge M. Fundamentals of Polymer Degradation and Stabilization. 2nd ed. London: Elsevier Applied Science; 1992